HHS Public Access

Author manuscript

Neuroimage. Author manuscript; available in PMC 2015 October 15.

Published in final edited form as:

Neuroimage. 2014 October 15; 100: 237–243. doi:10.1016/j.neuroimage.2014.05.081.

Reversal of cortical information flow during visual imagery as compared to visual perception

Daniela Dentico[1], **Bing Leung Cheung**[2], **Jui-Yang Chang**[2], **Jeffrey Guokas**[1], **Melanie Boly**[1,3], **Giulio Tononi**[1], and **Barry Van Veen**[2]

[1] Department of Psychiatry, University of Wisconsin - Madison, 6001 Research Park Blvd, Madison, WI 53719

[2] Department of Electrical and Computer Engineering, University of Wisconsin – Madison, 1415 Engineering Drive, Madison, WI 53706

[3] Coma Science Group, Cyclotron Research Center and Neurology Department, University of Liège, Allée du 6 août n° 8, 4000 Liège, Belgium 4000

Abstract

The role of bottom-up and top-down connections during visual perception and the forming of mental images was examined by analyzing high-density EEG recordings of brain activity using two state-of-the-art methods for assessing the directionality of cortical signal flow: state-space Granger causality and dynamic causal modeling. We quantified the directionality of signal flow in an occipito-parieto-frontal cortical network during perception of movie clips versus mental replay of the movies and free visual imagery. Both Granger causality and dynamic causal modeling analyses revealed increased top-down signal flow in parieto-occipital cortices during mental imagery as compared to visual perception. These results are the first direct demonstration of a reversal of the predominant direction of cortical signal flow during mental imagery as compared to perception.

Keywords

Imagery; Perception; Top-down; Bottom-up; Granger causality; Dynamic causal modeling

Introduction

Visual mental imagery and perception share similar cortical representations (Cichy et al., 2012; Kosslyn, 2005; Pylyshyn, 2003). It has been proposed that, while brain forward connections convey information from the outside world, backward connections might have a

Corresponding Author: Barry Van Veen vanveen@engr.wisc.edu 3611 Engineering Hall 1415 Engineering Drive Madison, WI 53706 (608) 265-2488.
Daniela Dentico, dentico@wisc.edu Bing Leung Cheung, blpcheung@gmail.com Jui-Yang Chang, jchang38@wisc.edu Jeffrey Guokas, jeffreyguokas@gmail.com Melanie Boly, mboly@ulg.ac.be Giulio Tononi, gtononi@wisc.edu

dominant role during the forming of mental images in the absence of external bottom-up inputs (Ganis and Schendan, 2008; Ishai et al., 2000; Kalkstein et al., 2011; Kosslyn, 2005). Despite the relevance of top-down and bottom-up dynamics for the understanding of the generative mechanisms of visual mental representations (Corbetta and Shulman, 2002; Friston, 2002; Kosslyn, 2005), a direct quantitative comparison of the directionality of neural signal flow during visual perception and imagery is still missing.

In the present study, we exploited the temporal resolution of high-density electroencephalography (hdEEG) and two state-of-the-art causal modeling methods to measure cortical directed connectivity during visual perception and visual mental imagery. We hypothesized that during visual perception bottom-up connectivity from early visual areas to higher order cortices would be predominant; whereas during visual mental imagery, higher order areas would lead the recruitment of early visual cortices in a top-down manner. This idea is consistent with current notions of visual imagery and perception and with indirect experimental evidence (Ganis and Schendan, 2008; Ishai et al., 2000; Kalkstein et al., 2011; Kosslyn, 2005; Mechelli et al., 2004).

We quantified directed connectivity from hdEEG recordings by means of two complementary approaches: Granger causality (GC) and dynamic causal modeling (DCM) (Friston et al., 2013). GC measures how the past signal of one region improves the prediction of the present signal of another region. We inferred cortical GC in the context of a state-space multivariable autoregressive (MVAR) model developed by our team (Cheung et al., 2010). DCM for cross-spectral densities (CSD) uses a nonlinear generative neural model (Friston et al., 2012) to estimate phase-delays and power spectrum contents and infer directionality of connectivity between modeled cortical areas. Both methods have been used in the neuroimaging literature to estimate cortical activity directionality. In the absence of a gold standard (Friston et al., 2013), and because of the different assumptions of GC and DCM, we opted to use both methods to increase confidence in the results.

We recorded brain activity while subjects engaged in both visual perception and imagery under two complementary paradigms: a short movie paradigm, designed to have the highest similarity between the content of visual imagery and that of perception, and a daydreaming paradigm, intended to optimize the spontaneous flow of visual processing during mental imagery. Our experimental design includes two ways of generating visual perception or imagery: 1) the replay of an extrinsically generated percept, and 2) an intrinsically generated series of mental images followed by an independently generated percept. We deliberately chose this strategy to confirm the generality of our results, irrespective of how the perceptual content was generated.

We directly compared long-range directed connectivity during imagery and perception in a cortical network comprised of an early visual area, the inferior occipital gyrus (IOG), and two higher order cortices, the superior parietal lobule (SPL), and the dorsolateral prefrontal cortex (PFC, Brodmann area 46) (Figure 1). Each of these cortical regions, or nodes of the network, is known to be activated during both perception and imagery tasks (Ganis and Schendan, 2008; Gardini et al., 2009; Harrington et al., 2007; Ishai et al., 2000).

Methods

1. Participants

Twenty healthy right-handed volunteers (10 females and 10 males, mean age of 27.3 years, range from 22 to 38 years) took part in this study. Written informed consent was obtained from each subject following medical screening. Imagery skills were screened using the 32 items of the Vividness of Visual Imagery Questionnaire 2 (VVIQ2, (Cui et al., 2007; Marks, 1995)), for both eyes closed and eyes open imagery. Only subjects with a minimum averaged score of 3 on a 5 points scale (average 3.8, range from 2.9 to 4.9) participated to the study. The subjects were requested to have a good night of sleep and not to consume caffeine the morning before the experiment. All procedures were approved by the University of Wisconsin Institutional Review Board.

2. Experimental design

Participants arrived at the laboratory between 9 a.m. and 12 p.m. for set-up, then started the experiment. The experimental paradigm combined resting state, perception of movies and visual imagery conditions (Figure 2). The order of the eyes closed and eyes open baseline and imagery conditions throughout both experimental paradigms were counterbalanced among subjects.

2.1. Resting state baseline—At the beginning of the experiment, 5 to 6 minutes of resting state EEG were recorded during both eyes closed and eyes open conditions. Additional baseline sessions were performed after each paradigm in a subset of 6 subjects. These additional data were not further analyzed in the context of this study. During the resting state, participants were given the instruction to avoid producing vivid visual imagery.

2.2.1. Visual Perception - Sims3 paradigm: Participants were shown 6 short movies of about 1 min length. This duration was chosen based on preliminary observations of a good match between the time spent in replaying the movie plot and its actual duration. The movies were obtained from The Sims3, a life-simulation computer game (average duration of 56 s, range from 50 to 63 s, total duration of 5 min and 36 s).

2.2.2. Visual Imagery - Sims3 paradigm: Following each presentation of the Sims3 movies, the participants were instructed to mentally replay the movie both with eyes closed and with eyes open, as vividly and in as much detail as they could, focusing on the shapes, colors, texture, and movements previously perceived. The subject signaled the start and the end of the imagery performance orally. The imagery performance fell within the 5 min window of persistence of iconic memory of sensory traces (Ishai and Sagi, 1995). The vividness of the imagery for each segment was rated on a 5 points scale (drawn from the VVIQ2 used for screening the imaginative skills of the participants).

2.3.1. Visual Imagery - Daydreaming paradigm: Participants were requested to imagine traveling with a magic bike they rode to a destination of their choice, including the depth of the ocean or the sky, without the need to pedal. They were instructed to focus vividly on the details (shapes, colors, textures, and movements) of the scenarios they were imagining. The

daydreaming imagery was performed both with eyes closed and with eyes open, for 5-6 min each.

2.3.2. Visual Perception - Daydreaming paradigm: A silent movie with naturalistic scenes was shown (duration of 5 min and 23 sec). This visual perception was performed after the mental imagery daydreaming session described above.

2.4. Visual Imagery ratings—In both paradigms, the vividness of the imagery was rated on a 5 points scale (VVIQ2). The average subjective rating for the mental replay of short movies (The Sims 3 paradigm) and for the free-guided imagery (daydreaming paradigm) was 3.7 (range from 3 to 4.5) and 4.2 (range from 3 to 5), respectively.

3. Data acquisition and analysis

The participants were seated in a dim and quiet room at 70 cm from the screen, with a headrest. The movies were shown in a 10.4 wide x 8.4 high cm frame at the center of the screen. Participants were instructed to limit eye movements during both eyes closed and eyes open recordings. A central fixation cross was displayed throughout the perception and imagery runs a well as during the resting baselines. The start and end of each short movie were synchronized with the EEG recordings.

3.1. Data acquisition—High-density electroencephalography (256 electrodes, Electrical Geodesics Inc., Eugene, OR) was recorded with vertex referencing, at a 500 Hz sampling frequency, using the NetStation software (Electrical Geodesics Inc., Eugene, OR).

3.2. Preprocessing—EEG data were analyzed using the NetStation software and MATLAB (The MathWorks Inc., Natick, MA). The data were average referenced. Three distinct stages of preprocessing were applied to the data. The first stage was for the purpose of artifact rejection using ICA. The data were bandpass filtered (cut off frequencies 0.5 Hz and 58 Hz) to eliminate baseline shifts and electrical line noise. The first and last 4 seconds of each data segment was then removed to avoid filter start-up transients. Bad channels and artefactual EEG segments were identified visually and removed. Next, eye movements, eye blinks, muscular activity and heartbeat artifacts were removed using temporal ICA (EEGLab, UCSD) (Onton and Makeig, 2006). The ICA-cleaned data were then further preprocessed specifically for either the MVAR/GC or DCM analyses.

The GC analysis was based on downsampling the ICA-cleaned data by a factor of six to an 83 Hz sampling rate. The downsampling process involved low pass filtering the data (40 Hz stopband edge) to prevent aliasing followed by discarding samples. Our interest is in behavior below 30 Hz, and higher than Nyquist sampling rates lead to large MVAR filter orders, which complicates model estimation. The downsampled data were then high pass filtered (2.5 Hz stopband) to remove low-frequency artifacts. The data at the start of each record contaminated by filter start-up transients was removed. The data was then segmented into 4-second epochs. GC analyses assume that the data is covariance stationary. Thus, stationarity and Gaussianity tests were performed on each 4-second epoch using two-sample and single-sample Kolmogorov-Smirnov goodness-of-fit hypothesis tests respectively. Only the epochs that met both criteria were used in the GC analysis.

The DCM analysis downsampled the ICA-cleaned data by a factor of 2 to a 250 Hz sampling rate and also operated on 4-second epochs. The SPM software projected the sensor data at each time point onto eight spatial modes obtained as the principal components of the downsampled data. The DCM analysis was performed on the 4-25 Hz band to correspond to the same frequency range studied using broadband GC.

3.3. Directed connectivity measurements

3.3.1. Source regions and model fitting: The choice of regions in our model was based on a priori knowledge of their involvement in various aspects of visual processing. We chose to include the bilateral inferior occipital gyri (IOG), superior parietal lobules (SPL), and dorsolateral prefrontal cortices (PFC, cortical patch limited to Brodmann area 46) (Figure 1a) (Ishai et al., 2000; Mechelli et al., 2004). The fronto(F)-parieto(P)-occipital(O) networks employed are shown in Figure 1 on a cortical surface in Montreal Neurological Institute (MNI) normalized space. The regions used in the DCM analysis closely corresponded to the center of mass of regions used for the GC results. Each DCM region corresponds to a cortical patch of 16 mm radius (Daunizeau et al., 2009). The MNI coordinates of the center of mass for right IOG (27,−97,-10), left IOG (−27,−97,−10), right SPL (26,−64,56), left SPL (−26,−64,56), right PFC (48,40,20), and left PFC (−48,40,20) were based on previous reports of fMRI activation of these regions during imagery and perception (Ganis et al., 2004; Gardini et al., 2009; Harrington et al., 2007)

Both state-space GC and DCM employ an observation model to describe how the neural activity from these cortical regions maps to the observed signal measured at the scalp. The observation model is based on average-referenced leadfields corresponding to the dipoles in the cortical regions of interest. The leadfields were computed using standardized electrode positions defined by the sensor net geometry relative to a standard brain that is coregistered with the MNI brain. That is, we did not use subject specific lead fields and brain regions. The leadfields used in the GC analysis were computed within the Geosource software package (Electrical Geodesics Inc., Eugene, OR) using a four-shell (brain, cerebrospinal fluid, skull and scalp surfaces) spherical head model. In this model, dipoles are constrained to 7-mm cortical voxels of the average MNI brain and consist of three orthogonal source orientations (xyz). This results in a parcellation of the cortex by 2447 dipoles. Leadfields in the DCM analysis were computed within SPM8 using a boundary element method applied to the MNI template after parcellation of the cortical surface using 3004 dipoles (Fuchs et al., 2001).

The GC analysis is based on an MVAR generative model for the activity in each cortical region (Cheung et al., 2010), while the generative model used in the DCM analysis represents neuronal interactions with a neural mass model (Pinotsis et al., 2012). The measured scalp data is described by the combined observation equation and cortical generative model in both cases. The unknown parameters of the observation equation and cortical generative models were estimated simultaneously using either a maximum likelihood (MVAR) or Bayesian (DCM) approach (Cheung et al., 2010; Friston et al., 2003).

3.3.2. Granger causality: Connectivity estimates were inferred using a state-space MVAR model (Cheung et al., 2010). In this approach, a state equation representing the cortical MVAR model is combined with an observation equation describing the EEG measurement of cortical signals. In contrast to conventional approaches that estimate source reconstructed signals and then estimate MVAR model parameters in two different steps (Barrett et al., 2012), we optimized the MVAR and other state-space model parameters simultaneously from the measured data. Specifically, we directly estimated the MVAR model parameters in the state equation, the unknown spatial activity distribution components in the observation equation, and the spatial covariance matrix of the observation noise from the measured EEG signal. The resulting MVAR parameters describe the cortical network, that is, network interactions in source space, but are estimated directly from scalp recordings via an expectation-maximization algorithm. This integrated approach is more robust to experimental noise, as compared to classical two-stage approaches (Cheung et al., 2010).

Each region of interest is represented as a cortical patch. The scalp signal generated by the patch activity is modeled as a weighted combination of dipoles leadfields within the patch. Here the weights describe the unknown spatial distribution of activity in the patch. Since concatenated leadfields from adjacent dipoles are inherently low rank (Limpiti, et al., 2006), we used a singular value decomposition of the patch leadfields to approximate this representation for the activity in each patch with three known spatial components and three unknown coefficients approximating the spatial activity distribution. The unknown coefficients representing the spatial activity in each patch are estimated from the data. Thus, each patch is represented by a single time series (Cheung, et al. 2010) and a six-region MVAR model relates the activity of the six cortical time series in the network. Brain activity that is not described by the six regions is thus considered observation noise.

A MVAR model order of 20 was selected using the Bayesian information criterion (BIC), based on the maximum observed data log-likelihood (Akaike, 1978). An expectation-maximization algorithm developed in (Cheung et al., 2010) was employed to obtain maximum-likelihood estimates of the MVAR model parameters, the observation noise covariance matrix, and the spatial activity patterns within each region.

The estimated six-region MVAR models were used to evaluate cortical conditional GC (Geweke, 1982) between occipital, parietal, and frontal regions of interest, after pooling the source activity implied by the MVAR model across hemispheres. This corresponds to evaluation of conditional GC between three “super” nodes, each of which involves activity in two hemispheres. The conditional GC from region A to B given C is defined as the ratio of the error variance when predicting the time series of B using its own past and the past of region C time series to that using its own past and the past of regions C and A time series. The conditional GC metric was computed bidirectionally in the 4-25 Hz frequency range, using the frequency decomposition approach described in (Chen et al., 2006), between frontal and parietal, frontal and occipital, parietal and occipital regions.

Data-driven frequency ranges of interest for computing broadband GC were selected post-hoc, based on the distribution of the cortical power spectral density (PSD) as derived from the MVAR model parameters. The PSD vectors for each subject, condition, and cortical

region, were normalized to their maximum value and then averaged. The troughs of the averaged PSD were used to delimit the windows of the frequency ranges of interest. Specifically the integral of GC estimates was computed across the 8.8-12.7 Hz range for the alpha band and across the 16.3-23.9 Hz range for the beta band. The 8.8-12.7 Hz band contained one peak at 10.1 Hz, the 16.3-23.9 Hz band contained two peaks at 18.1 and 21.6 Hz respectively. The conditional GC estimates in the bottom-up direction were subtracted from the top-down estimates to obtain differential top-down – bottom-up estimates of the connectivity measures.

3.3.3. Dynamic causal modeling: DCM for CSD models EEG time-series as the response of a network of sources, where each source corresponds to a neural mass model of several subpopulations responding to endogenous fluctuations. The model encompassed the cortical areas described above (bilateral IOG, SPL, PFC), connected by forward, backward and lateral connections as described in Figure 1b (right). Specifically, we used a canonical microcircuit (CMC) neural mass model containing four populations of neurons in the cortical column: excitatory interneurons, inhibitory interneurons and two populations of pyramidal cells (Pinotsis et al., 2012). The spiny stellate cells receive external inputs, and the pyramidal cells are long-range projection neurons, with the supragranular layers originating forward driving connections and the infragranular layers projecting backward modulatory connections. This model structure is biologically plausible (Buffalo et al., 2011; Roopun et al., 2006; Salin and Bullier, 1995) and allows parameterization of both interlayer and inter-areal interactions (Pinotsis et al., 2012). In DCM for cross-spectral density responses, neuronal dynamics are assumed driven by endogenous neuronal fluctuations with unknown but parameterized spectral density. This assumption is particularly suitable to conditions in which we don't model exogenous stimuli, as when studying brain states under steady-state conditions. (Moran et al., 2009). The endogenous neuronal fluctuations are represented as a mixture of pink and white noise. Hence, we used complex spectra to estimate phase-delays at the source level from observed EEG time-series. Model estimation involves fitting the predicted cross-spectral density between any two channels given the parameters of the observation model and the neuronal state equations, to the observed data features (Moran et al., 2009).We derived the estimates of connectivity strength from the DCM parameters. The condition-specific changes in connectivity - as estimated by DCM - were then used to summarize asymmetries in coupling for each subject. This procedure is theorized to enable an accurate estimation of bidirectional coupling strength (Friston et al., 2012). We allowed the parameters represented in Figure 1b to be modulated between baseline and cognitive states at the level of forward and backward connections (Friston et al., 2003).

The SPM8 version of the Statistical Parametric Mapping software was used to identify the DCM. Within SPM8 we explicitly set the data features as CSD, the neural model as CMC, the latent connectivity matrix A and the induced connectivity matrix B, as well as the frequency range of interest and the segment length. All other parameters, including the prior expectations for the coupling parameters between sources and within the cortical column representing each source, were estimated within SPM from the data.

3.3.4. Relationship between GC and DCM connectivity measures: Both GC and DCM provide estimates of directed coupling; however they are practically and conceptually distinct: GC can be regarded as a measure of statistical dependence between signals that is causal in the sense of temporal precedence. Put simply, GC represents the proportion of variance explained in a target node by conditioning on the history of a source node. In our implementation (Cheung et al., 2010; Geweke, 1982), we have expressed GC as a function of frequency and have evaluated directed coupling on a regular grid of frequencies and summed over frequency bins to quantify broadband coupling strength in a particular band. In contrast, DCM represents the effective connectivity using a single number - a coupling or rate constant between neural populations in the equations representing the DCM. In what follows, we use the GC and DCM connectivity measures as summary statistics and test for asymmetries in these measures using classical inference.

4. Statistical analyses

Statistical analyses on conditional GC and DCM estimates of effective connectivity were performed with STATISTICA 6.1 (StatSoft. Inc., Tulsa, OK, USA) and MATLAB software. For GC, statistical analyses were carried on the difference between top-down and bottom-up estimates after baseline subtraction. For DCM, the eyes-open baseline was used as a reference, and the eyes-closed baseline was then subtracted from the eyes-closed imagery. This approach was taken to account for baseline eyes open and closed connectivity with both methods. Statistical analyses were then performed on these baseline-subtracted differential top-down – bottom-up DCM estimates of coupling strength. Statistical analysis was organized according to a factorial (a × b × c × d) design for both GC and DCM. Factor a, the *paradigm* factor, had 2 levels (extrinsic and intrinsic, corresponding to Sims3 and daydreaming paradigms, respectively). Factor b, the experimental *condition* factor, had 3 levels (eyes closed imagery, eyes open imagery, and perception). Factor c, the *edge* factor ('edge' corresponds to a connection in our network model), had 3 levels (FP, FO, and PO). Factor d, the *frequency* factor, had 2 levels (alpha and beta) for conditional GC and was not represented for d DCM.

Results were evaluated by means of repeated measures univariate analysis of variance (rmANOVA). Significance levels were pre-set at $p < 0.05$. Greenhouse-Geisser corrections for violation of sphericity were applied to significance levels and degrees of freedom. Owing to the presence of a significant two-way interaction (*condition*edge*), the preplanned comparisons, imagery *vs* perception, and eyes-closed *vs* eyes-open imagery conditions were carried out independently for each edge by means of paired t-tests. All results were corrected for multiple comparisons using False Discovery Rate (Nichols and Hayasaka, 2003).

Results

GC

For GC, a repeated-measures ANOVA (rmANOVA) compared differential [top-down – bottom-up] GC estimates along the edges of the graph defined by the cortical nodes during imagery as compared to perception. The GC values for the following three edges were evaluated in both directions: occipito-parietal, parieto-occipital, occipito-frontal, fronto-

occipital, parieto-frontal, fronto-parietal. The memory of the MVAR model for our data, selected using a Bayesian information criterion, used signal latencies of up to 250 ms. The results of this analysis revealed a significant interaction between the condition (imagery versus perception) versus the edge (occipito-parietal, occipito-frontal and parieto-frontal) factors ($F_{23,433} = 6.76$, $p = 0.004$), with no difference between experimental paradigms. Preplanned comparisons (imagery *vs* perception, and eyes-closed *vs* eyes-open imagery) confirmed significantly more top-down flow from SPL to IOG during imagery as compared to perception ($t_{19} = 3.32$, $p = 0.0036$; false discovery rate corrected, Figure 3). There was no difference between the two imagery conditions.

DCM

A repeated-measures ANOVA was also performed on the differential [top-down – bottom-up] DCM estimates of directed connectivity during imagery versus perception. The DCM results were also baseline-subtracted and estimates were pooled over hemispheres. Consistent with the GC result, we confirmed the presence of a significant interaction between *condition* and *edge* factors ($F_{14,264} = 3.48$, $p = 0.0249$; respectively), with no difference between experimental paradigms. Preplanned comparisons, computed following the same design as for the conditional GC estimates, identified a reversal of flow during imagery versus perception in the parieto-occipital connection ($t_{19} = 4.00$, $p = 0.0008$; false discovery rate corrected, Figure 4). This connection showed a prevalent top-down flow in imagery and a prevalent bottom-up flow in perception. Once again, there was no difference between the imagery conditions.

Discussion

Our main finding is a reversal of neural signal flow in parieto-occipital cortices during visual imagery as compared to perception. This study provides the first quantitative demonstration of this change in the predominant direction of cortical interactions, a finding that is consistent with current notions about visual imagery and perception (Kosslyn, 2005). These results were obtained thanks to the excellent temporal resolution of hdEEG and two newly developed state-of-the-art directional connectivity estimation methods, state-space based GC and DCM. The fact that we obtained consistent results using these two very different methods strongly increases the confidence in the present findings.

Two experimental paradigms, mental replay of short movies and free guided imagery followed by perception of naturalistic scenes, were explicitly chosen to capture underlying mechanisms involved in perception and imagery. The mental replay paradigm was designed to closely match the content of imagery and that of perception, while the free imagery-natural scene perception paradigm was intended to optimize the spontaneous flow of visual mental imagery. While these two paradigms differ in several respects, including attentional effort and memory load, with respect to directed connectivity they were similar to each other. Thus, the observed differences in directed connectivity are likely due to common differences between imagery and perception, rather than to specific features of the two imagery tasks.

These results are in line with previous studies suggesting a differential recruitment of visual pathways during imagery versus perception. A study applying DCM to fMRI time-series (Mechelli et al., 2004) showed bottom-up influences from occipital to temporo-occipital category selective regions during perception of simple objects, as opposed to top-down influences from prefrontal cortex to the same regions during imagery. However, the temporal resolution of fMRI precluded the use of temporal delays to estimate directional connectivity in the model (Friston et al., 2013). Moreover, this study did not directly compare imagery and perception conditions. Another study showed that changes in amplitude of the N170 visual event related potential during imagery versus perception could be interpreted as evidence for increased top-down processes during imagery (Ganis and Schendan, 2008). Facilitatory effects of mental imagery on subsequent perception, likely mediated by top-down influences of higher-order areas on visual cortices, have also been described (Pearson et al., 2008). Finally, our findings are in line with a recent magnetoencephalography DCM study (van Wijk et al., 2013), suggesting increased beta top-down motor cortex modulation of gamma stimulus-induced activity in occipital areas during mental imagery trials that have slow reaction times, and thus presumably require more cognitive effort. However, the study in (van Wijk et al., 2013) did not directly compare perception and imagery.

The directed connectivity methods employed here, state-space based GC and DCM exploit the high temporal resolution of EEG and allowed us to demonstrate consistent changes in the predominant direction of neuronal interactions between visual imagery and visual perception. While the overall results concerning directionality were similar with both methods, there are inherent differences in these models. The MVAR models used for GC analyses were based on a temporal memory of 20 time bins, that is, latencies of up to 240 ms, which is the time scale of conscious cognition (Lehmann et al., 1998; Tononi, 2012). In contrast, in DCM there is an explicit conduction delay that parameterizes the interactions between areas. DCM priors for inter-area latencies are around 20 milliseconds - though they are then modified during model estimation. Another difference between the MVAR GC (Cheung et al., 2010) and DCM for CSD (Moran et al., 2009; Pinotsis et al., 2012) approaches is that the MVAR GC model does not explicitly represent nonlinear interactions between brain regions (Friston, 2000). Furthermore, the MVAR model assumes that the innovations are independent in time and therefore have a uniform spectrum. This contrasts with the colored neuronal innovations estimated by DCM (Friston et al., 2013). The MVAR model assumes linear interactions, while the DCM model is based on neurobiologically inspired nonlinear interactions. The comparison of imagery and perception conditions rests upon separate estimations of model parameters for GC, while for DCM, a subset of parameters or connections were allowed to change with condition and all the other parameters are held constant. Also, the DCM analysis was performed after projecting the ICA-cleaned data onto eight spatial modes; the GC analysis was performed using all of the spatial modes that remained after ICA. Despite these dissimilarities, an increase in top-down connectivity during imagery was found in parieto-occipital regions using both techniques.

Neither GC nor DCM were able to identify statistically significant differences in frontal connectivity. Since the results for the frontal connections were not statistically significant in any of the cases in this study, it is inappropriate to attempt to draw conclusions from them.

We suspect that the lack of significance may be due to the insufficiency of the unimodal visual paradigm to distinctly recruit a significant level of activity in a known multimodal region such as the dorsolateral prefrontal cortex. Frontal cortices have been posited to backwardly activate mental representation in topographically organized visual cortices on the basis of information stored in memory (Kosslyn, 2005). Specifically, the dorsolateral prefrontal cortex has been shown to be involved in visual processing during both visual imagery and perception (Ganis and Schendan, 2008; Harrington et al., 2007). It is also likely that inadequate signal to noise ratio associated with frontal activity would make it difficult to draw consistent conclusions based on scalp data. Further investigations will be required to clarify the directionality of the involvement of the frontal lobes during visual imagery and perception.

Likewise, we cannot exclude that differences between the two experimental paradigms tested in this study, such as possible imbalances in cognitive load, could represent potential confounds in the interpretation of the results. Further experiments that exploit active paradigms to test the effect of cognitive load on directed connectivity during imagery and perception might resolve this ambiguity.

Note that we are reporting differential [top-down – bottom-up] directed connectivity estimates. Both forward and backward connections are present, but the effect of imagery is to increase the strength of backward connections relative to forward connections. This is in line with the notion that reciprocal or recursive connections are believed to subserve conscious cognition (Friston, 2000; Tononi et al., 1992). In short, the results suggest a set-dependent change in the asymmetry of forward and backward connections as opposed to a categorical reversal of unidirectional information flow.

The analysis presented here does not model all the possible brain areas involved in perception and imagery, but studies a subset of primary areas. Accounting for all possible cortical regions is not currently practical using any analysis method. Hence, our results should be interpreted in the sense of equivalency. The equivalent direction of the neural flow in the dorsal visual pathway, after accounting for the baseline connectivity, is more top-down during imagery and more bottom-up during perception, regardless of whether there is only direct interaction between the parietal and occipital regions as modeled, or whether intermediate unmodeled nodes are involved, for example, relaying information.

Finally, the consistency between the results obtained with state-space based GC and DCM methods provides strong evidence for reversal of the net direction of the neural signal flow along the visual dorsal stream between visual imagery and perception, even though both feedforward and feedback pathways are most likely involved in generating both perceived and imagined visual representations. This result opens the way to applying similar approaches to other conditions such as dreaming, where it is still unclear whether visual or other sensory representations are generated based primarily on bottom-up or top-down processing (Nir and Tononi, 2010).

Acknowledgements

This research was supported in part by the McDonnell Foundation (Tononi) and by the National Institute of Biomedical Imaging and Bioengineering under grant R21EB009749 (Van Veen). Melanie Boly is Postdoctoral Research Fellow at the Belgian National Fund for Scientific Research. We thank Corinna Zennig for editing the movies, and Rosalyn Moran for assistance with the DCM analyses. This research was performed using resources and the computing assistance of the UW-Madison Center For High Throughput Computing (CHTC) in the Dept of Computer Sciences. The CHTC is supported by UW-Madison and the Wisconsin Alumni Research Foundation, and is an active member of the Open Science Grid, which is supported by the National Science Foundation and the U.S. Department of Energy's Office of Science. The authors declare no competing financial interests.

References

Akaike H. A Bayesian analysis of the minimum AIC procedure. Annals of the Institute of Statistical Mathematics. 1978; 30:9–14. 30, 9–14.

Barnett L, Seth AK. Behaviour of Granger causality under filtering: theoretical invariance and practical application. J Neurosci Methods. 2011; 201:404–419. [PubMed: 21864571]

Barrett AB, Murphy M, Bruno MA, Noirhomme Q, Boly M, Laureys S, Seth AK. Granger causality analysis of steady-state electroencephalographic signals during propofol-induced anaesthesia. PLoS One. 2012; 7:e29072. [PubMed: 22242156]

Buffalo EA, Fries P, Landman R, Buschman TJ, Desimone R. Laminar differences in gamma and alpha coherence in the ventral stream. Proc Natl Acad Sci U S A. 2011; 108:11262– 11267. [PubMed: 21690410]

Chen Y, Bressler SL, Ding M. Frequency decomposition of conditional Granger causality and application to multivariate neural field potential data. J Neurosci Methods. 2006; 150:228–237. [PubMed: 16099512]

Cheung BL, Riedner BA, Tononi G, Van Veen BD. Estimation of cortical connectivity from EEG using state-space models. IEEE Trans Biomed Eng. 2010; 57:2122–2134. [PubMed: 20501341]

Cichy RM, Heinzle J, Haynes JD. Imagery and perception share cortical representations of content and location. Cereb Cortex. 2012; 22:372–380. [PubMed: 21666128]

Corbetta M, Shulman GL. Control of goal-directed and stimulus-driven attention in the brain. Nat Rev Neurosci. 2002; 3:201–215. [PubMed: 11994752]

Cui X, Jeter CB, Yang D, Montague PR, Eagleman DM. Vividness of mental imagery: individual variability can be measured objectively. Vision Res. 2007; 47:474–478. [PubMed: 17239915]

Daunizeau J, Kiebel SJ, Friston KJ. Dynamic causal modelling of distributed electromagnetic responses. Neuroimage. 2009; 47:590–601. [PubMed: 19398015]

Friston K. Functional integration and inference in the brain. Prog Neurobiol. 2002; 68:113–143. [PubMed: 12450490]

Friston K, Bastos A, Litvak V, Stephan KE, Fries P, Moran RJ. DCM for complex-valued data: cross-spectra, coherence and phase-delays. Neuroimage. 2012; 59:439–455. [PubMed: 21820062]

Friston K, Harrison L, Penny W. Dynamic causal modelling. Neuroimage. 2003; 19:1273– 1302. [PubMed: 12948688]

Friston K, Moran R, Seth AK. Analysing connectivity with Granger causality and dynamic causal modelling. Curr Opin Neurobiol. 2013; 23:172–178. [PubMed: 23265964]

Friston KJ. The labile brain. I. Neuronal transients and nonlinear coupling. Philos Trans R Soc Lond B Biol Sci. 2000; 355:215–236. [PubMed: 10724457]

Fuchs M, Wagner M, Kastner J. Boundary element method volume conductor models for EEG source reconstruction. Clin Neurophysiol. 2001; 112:1400–1407. [PubMed: 11459679]

Ganis G, Schendan HE. Visual mental imagery and perception produce opposite adaptation effects on early brain potentials. Neuroimage. 2008; 42:1714–1727. [PubMed: 18674625]

Ganis G, Thompson WL, Kosslyn SM. Brain areas underlying visual mental imagery and visual perception: an fMRI study. Brain Res Cogn Brain Res. 2004; 20:226–241. [PubMed: 15183394]

Gardini S, Cornoldi C, De Beni R, Venneri A. Cognitive and neuronal processes involved in sequential generation of general and specific mental images. Psychol Res. 2009; 73:633– 643. [PubMed: 18987882]

Geweke J. Journal of the American Statistical Association . Measurement of Linear Dependence and Feedback Between Multiple Time Series. 1982; 77:304–313.

Harrington GS, Farias D, Davis CH, Buonocore MH. Comparison of the neural basis for imagined writing and drawing. Hum Brain Mapp. 2007; 28:450–459. [PubMed: 16944477]

Ishai A, Sagi D. Common mechanisms of visual imagery and perception. Science. 1995; 268:1772–1774. [PubMed: 7792605]

Ishai A, Ungerleider LG, Haxby JV. Distributed neural systems for the generation of visual images. Neuron. 2000; 28:979–990. [PubMed: 11163281]

Kalkstein J, Checksfield K, Bollinger J, Gazzaley A. Diminished top-down control underlies a visual imagery deficit in normal aging. J Neurosci. 2011; 31:15768–15774. [PubMed: 22049420]

Kosslyn SM. Mental images and the Brain. Cogn Neuropsychol. 2005; 22:333–347. [PubMed: 21038254]

Lehmann D, Strik WK, Henggeler B, Koenig T, Koukkou M. Brain electric microstates and momentary conscious mind states as building blocks of spontaneous thinking: I. Visual imagery and abstract thoughts. Int J Psychophysiol. 1998; 29:1–11. [PubMed: 9641243]

Limpiti T, Van Veen BD, Wakai RT. Cortical patch basis model for spatially extended neural activity. IEEE Trans Biomed Eng. 2006; 53:1740–54. [PubMed: 16941830]

Marks DF. New directions for mental imagery research. Journal of Mental Imagery. 1995; 19:153–167.

Mechelli A, Price CJ, Friston KJ, Ishai A. Where bottom-up meets top-down: neuronal interactions during perception and imagery. Cereb Cortex. 2004; 14:1256–1265. [PubMed: 15192010]

Moran RJ, Stephan KE, Seidenbecher T, Pape HC, Dolan RJ, Friston KJ. Dynamic causal models of steady-state responses. Neuroimage. 2009; 44:796–811. [PubMed: 19000769]

Nichols T, Hayasaka S. Controlling the familywise error rate in functional neuroimaging: a comparative review. Stat Methods Med Res. 2003; 12:419–446. [PubMed: 14599004]

Nir Y, Tononi G. Dreaming and the brain: from phenomenology to neurophysiology. Trends Cogn Sci. 2010; 14:88–100. [PubMed: 20079677]

Onton J, Makeig S. Information-based modeling of event-related brain dynamics. Prog Brain Res. 2006; 159:99–120. [PubMed: 17071226]

Pearson J, Clifford CW, Tong F. The functional impact of mental imagery on conscious perception. Curr Biol. 2008; 18:982–986. [PubMed: 18583132]

Pinotsis DA, Schwarzkopf DS, Litvak V, Rees G, Barnes G, Friston KJ. Dynamic causal modelling of lateral interactions in the visual cortex. Neuroimage. 2012; 66C:563–576. [PubMed: 23128079]

Pylyshyn Z. Return of the mental image: are there really pictures in the brain? Trends Cogn Sci. 2003; 7:113–118. [PubMed: 12639692]

Roopun AK, Middleton SJ, Cunningham MO, LeBeau FE, Bibbig A, Whittington MA, Traub RD. A beta2-frequency (20-30 Hz) oscillation in nonsynaptic networks of somatosensory cortex. Proc Natl Acad Sci U S A. 2006; 103:15646–15650. [PubMed: 17030821]

Salin PA, Bullier J. Corticocortical connections in the visual system: structure and function. Physiol Rev. 1995; 75:107–154. [PubMed: 7831395]

Tononi G. Integrated information theory of consciousness: an updated account. Arch Ital Biol. 2012; 150:56–90. [PubMed: 23165867]

Tononi G, Sporns O, Edelman GM. Reentry and the problem of integrating multiple cortical areas: simulation of dynamic integration in the visual system. Cereb Cortex. 1992; 2:310–335. [PubMed: 1422090]

Tucker DM, Waters AC, Holmes MD. Transition from cortical slow oscillations of sleep to spike-wave seizures. Clin Neurophysiol. 2009; 120:2055–2062. [PubMed: 19879188]

van Wijk BC, Litvak V, Friston KJ, Daffertshofer A. Nonlinear coupling between occipital and motor cortex during motor imagery: A dynamic causal modeling study. Neuroimage. 2013; 71C:104–113. [PubMed: 23313570]

Highlights

- We studied bottom-up and top-down connections during visual perception and imagery.
- A cortical occipito-parieto-frontal network was modeled from high-density EEG data.
- Our approach used both state-space Granger causality and dynamic causal modeling.
- Parieto-occipital directed connectivity reversed during imagery versus perception.
- This is the first quantitative demonstration of theorized connectivity reversal.

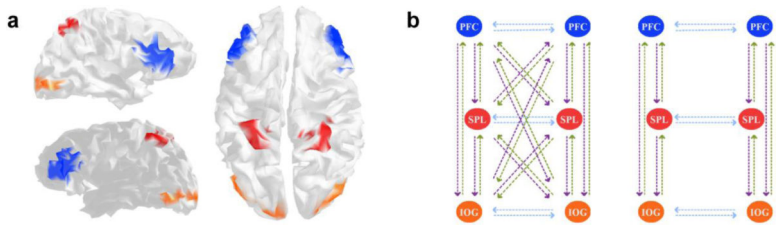

Figure 1.

Panel a. Regions of interest displayed on a cortical surface reconstruction of the average brain from the Montreal Neurological Institute (MNI). Orange, inferior occipital gyrus; red, superior parietal lobule; blue, Brodmann area 46, part of the dorsolateral prefrontal cortex. **Left.** Lateral views of the brain: right (top) and left (bottom). **Right.** Brain view from above. **Panel b.** Network representation of backward (violet), forward (green), and lateral (blue) latent connections included in the MVAR model used to compute GC (**left**) and the DCM (**right**). The MVAR models for the GC analyses were based upon the six nodes depicted. However, GC values were computed by pooling over right and left hemispheres. Consequently, we estimated GC on backward and forward connections grouping the homologous regions in both hemispheres to characterize three functional interactions between frontal, parietal, and occipital regions. In the DCM we only allowed condition-specific changes in the backward and forward connections, and then averaged estimates across hemispheres. IOG: inferior occipital gyrus; SPL: superior parietal lobule; PFC: BA46 in the dorsolateral prefrontal cortex.

Figure 2.

Experimental design. In The Sims3 or extrinsic paradigm, the participants were shown short clips from The Sims3 videogame and asked to replay them with their imagination as vividly and in as much detail as possible. In the daydreaming or intrinsic session, the participants were instructed to imagine traveling with a magic bike and to vividly focus on the details (shapes, colors, textures, movements) of the imagined scenarios. A movie with naturalistic scenes was then shown to match the daydreaming imagery. The order of eyes closed and open imagery and resting baseline was counterbalanced among participants. 256-Channel Geodesic Sensor Net image reproduced with permission from (Tucker et al., 2009).

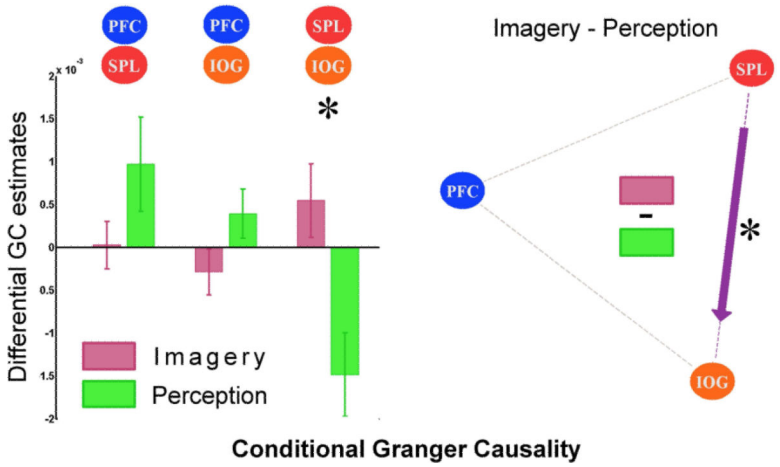

Figure 3.

Left. Bar graph of differential [top-down – bottom-up] estimates of directed connectivity in imagery (green) and perception (pink) after baseline-subtraction, as measured by GC. The daydreaming and Sims-3 paradigms are averaged together, as well as the eyes-closed and eyes-open imagery conditions. The alpha (8-13 Hz) and beta (16-24 Hz) bands are also averaged. The asterisk denotes the statistically significant difference Imagery *vs* Perception over subjects after false discovery rate correction. **Right.** Network representation of statistically significant differences in imagery minus perception. The arrow represents the direction of the net neural flow. IOG: inferior occipital gyrus; SPL: superior parietal lobule; PFC: BA46 in the dorsolateral prefrontal cortex.

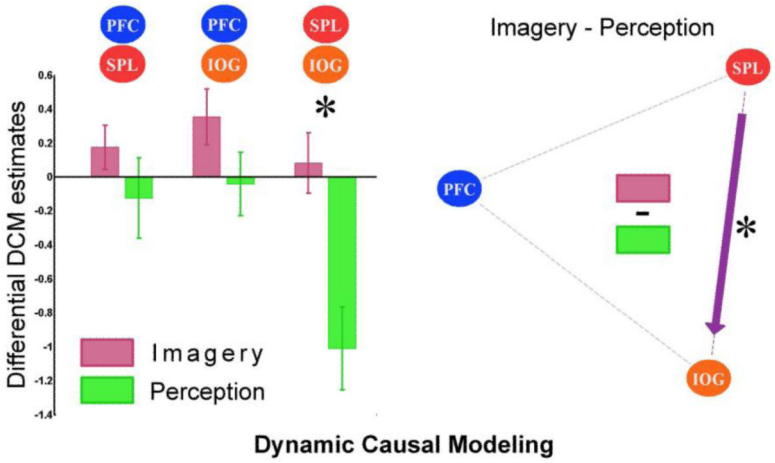

Figure 4.

Left. Bar graph of differential [top-down – bottom-up] estimates of directed connectivity in imagery (green) and perception (pink) after baseline-subtraction, as measured by DCM. The daydreaming and Sims-3 paradigms are averaged together, as well as the eyes-closed and eyes-open imagery conditions. The estimates are based upon the 4-25 hertz (broad band) data features used for the Granger causality analyses. The asterisk denotes the statistically significant difference Imagery *vs* Perception over subjects after false discovery rate correction.**Right.** Network representation of statistically significant differences in imagery minus perception. The arrow represents the direction of the net neural flow. IOG: inferior occipital gyrus; SPL: superior parietal lobule; PFC: BA46 in the dorsolateral prefrontal cortex.